PROCEEDINGS OF THE ROYAL SOCIETY A

rspa.royalsocietypublishing.org

Research

Article submitted to journal

Subject Areas:
wave motion, dispersion analysis, asymptotic theory

Keywords:
elastic periodic structures, dispersion, band-gaps, localisation, asymptotics, damage

Author for correspondence:
Michele Brun
e-mail: mbrun@unica.it

Dynamic response and localisation in strongly damaged waveguides

G. Carta[1,2], M. Brun[1,2] and A. B. Movchan[2]

[1]Dipartimento di Ingegneria Meccanica, Chimica e dei Materiali, Università di Cagliari, Italy
[2]Department of Mathematical Sciences, University of Liverpool, UK

In this paper, we investigate the formation of band-gaps and localisation phenomena in an elastic strip nearly disintegrated by an array of transverse cracks. We analyse the eigenfrequencies of finite, strongly damaged, elongated solids with reference to the propagation bands of an infinite strip with a periodic damage. Subsequently, we determine analytically the band-gaps of the infinite strip by using a lower-dimensional model, represented by a periodically-damaged beam in which the small ligaments between cracks are modelled as 'elastic junctions'. The effective rotational and translational stiffnesses of the elastic junctions are obtained from an ad hoc asymptotic analysis. We show that, for a finite frequency range, the dispersion curves for the reduced beam model agree with the dispersion data determined numerically for the two-dimensional elastic strip. Exponential localisation, boundary layers and standing waves in strongly damaged systems are discussed in detail.

1. Introduction

Localisation around defects in solids is of high importance in mathematical models of elastic Bloch waves as well as in practical applications of engineering designs. Localisation phenomena, in particular trapped modes appearing near defects, can occur in elastic structures with defects, cracks or discontinuities such as beams [1], plates [1–3] and micro-structured media [4–7]. In addition, the dynamic response of elongated solids with a distribution of crack-like defects is used in the practical evaluation of properties of composite body armour as well as protection sheets and windscreens of armoured vehicles.

Royal Society Publishing
Informing the science of the future

The earlier papers [8] and [9] present an efficient algorithm for the analysis of localised modes around crack-like defects distributed periodically in a bi-material delaminating system. A special feature of the problem is the singular perturbation analysis in the region around a crack, and the reduction to a lower-dimensional approximation. Higher-order terms in the asymptotics are studied in [10], which allow for a higher accuracy in the description of the dispersion properties of Floquet-Bloch waves existing within the periodic system with longitudinal cracks.

In the present paper, we are interested in the dynamic response of nearly disintegrating systems. Examples include elongated solids containing transverse cracks which have grown to the extent that the solid is close to disintegration into several disjoint subsets. Such models also arise in the engineering designs of long bridges, pipelines and conveyors as well as in slender systems such as skyscrapers. More specifically, several bridges and viaducts are designed as series of simply supported spans, sustained by piers. In correspondence of each pier, the spans are connected only by the upper deck. Therefore, the junction at the pier behaves like a cracked section where the ligament is represented by the depth of the upper deck. An example of such structure is shown in Fig. 1.

Figure 1. Railway viaduct in Piacenza, Italy (image taken from the website http://www.tensacciai.it, accessed on 31/01/2014). The structure is 5070 m long and consists of 150 prestressed concrete, simply supported spans. (Online version in colour.)

We note that a static singularly perturbed problem for a disintegrating elongated elastic solid containing a transverse crack is studied in [11] and [12] for longitudinal and transverse loads, respectively. These works present the derivation of a lower-dimensional model and an effective junction condition, which serves as the condition of decay for the boundary layer occurring in the vicinity of the cracked region. A comparison with numerical results relevant to the calculation of the first eigenfrequency of a simply supported plate with a crack in the middle section shows that the asymptotic model in [12] behaves well for deep cracks, while the model proposed in [13] works better for small cracks.

The dynamic behaviour at high frequencies of a diffusively damaged structure may exhibit surprising features. Fig. 2a includes an instance of a damaged bridge, which can be modelled as an elongated solid weakened by transverse cracks, as sketched in Fig. 2b. Fig. 2c shows typical eigenmodes of the elongated solid. The eigenmodes at the top and bottom of the figure are localised near one end of the structure and are characterised by a different decaying rate, while the eigenmode at the middle of the figure presents a typical standing wave pattern.

Standing waves and localisation in strongly damaged systems possess new features and require a substantial additional effort with respect to static computations. In this paper, we identify and study standing waves leading to localisation phenomena. We also show that damaged structures exhibit band-gaps, and we derive analytical estimates for the frequency ranges of such band-gaps.

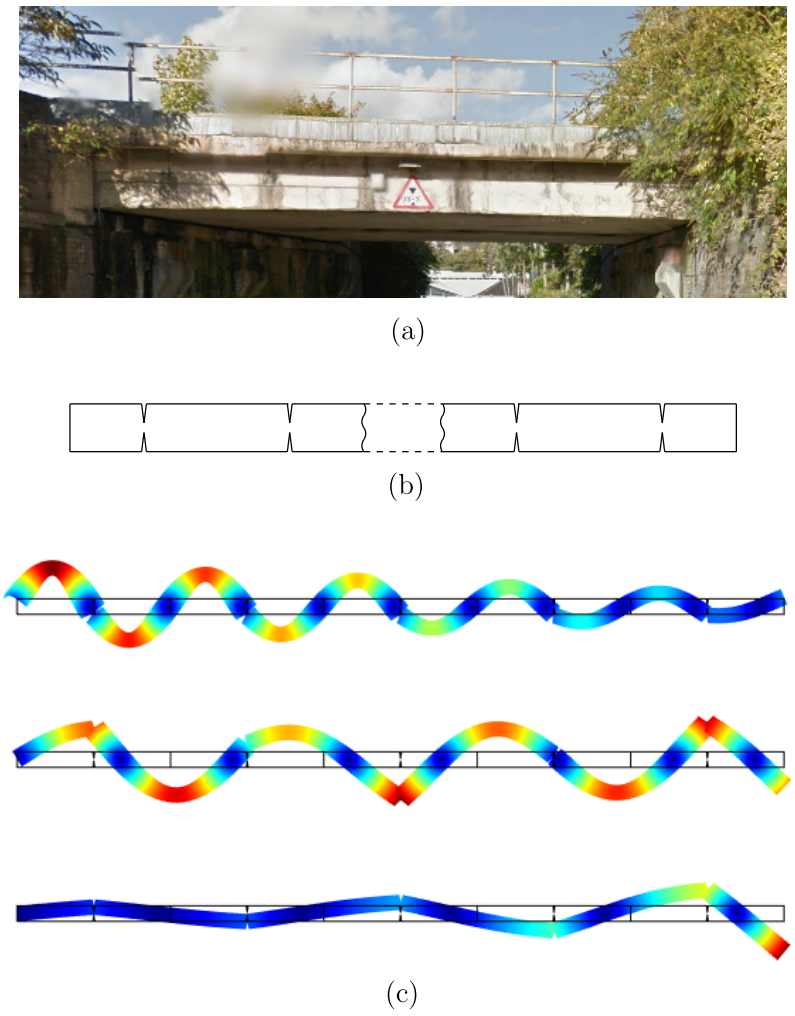

Figure 2. (a) Example of an elongated damaged structure: rail bridge over Westmoreland Road, Bath, UK (image taken from Google Maps Street View, website: https://maps.google.com/, retrieved on 31/01/2014); (b) schematic representation of a finite strip with equispaced cracks; (c) eigenmodes of the finite strip corresponding to three different frequencies (increasing from the bottom to the top of the figure), obtained from a finite element simulation in Comsol Multiphysics (version 4.3). (Online version in colour.)

The structure of the paper is as follows. In Section 2 we present the two-dimensional model of an elastic strip damaged at regular distances. We describe both a finite and an infinite periodic structure, and we derive numerically their dynamic responses. Section 3 is dedicated to the lower-dimensional model, which consists of a beam with periodic elastic connections that simulate the cracked sections. We revise the asymptotic method leading to the reduced model and then analyse the dispersion properties of the system obtained by means of the transfer matrix formalism. Simple analytical expressions for the frequency intervals of the propagation bands as a function

of the damage parameters are provided. Finally, we determine the dynamic range of applicability of the reduced model by comparison with the two-dimensional model of Section 2. Final remarks in Section 4 conclude the paper.

2. Two-dimensional strip model

We consider an elastic strip with a diffuse damage, represented by transverse cracks distributed at equal distances in the direction of the strip length. For the strip with finite dimensions, we determine numerically eigenfrequencies and eigenmodes for different values of the strip length. Then, we show that the frequency response of the finite strip is connected with the dispersion properties of a periodic strip of infinite length.

(a) Eigenfrequencies of the finite strip

A strip of finite dimensions is sketched in Fig. 3a. The length and the height of the strip are indicated by L and h, respectively. The distance between cracks is denoted by l. In the example of Fig. 3a, the strip is made of five identical units (or cells) of length l. One of these cells is drawn on an enlarged scale in Fig. 3b, where ρ_ϵ is the depth of the cracked section.

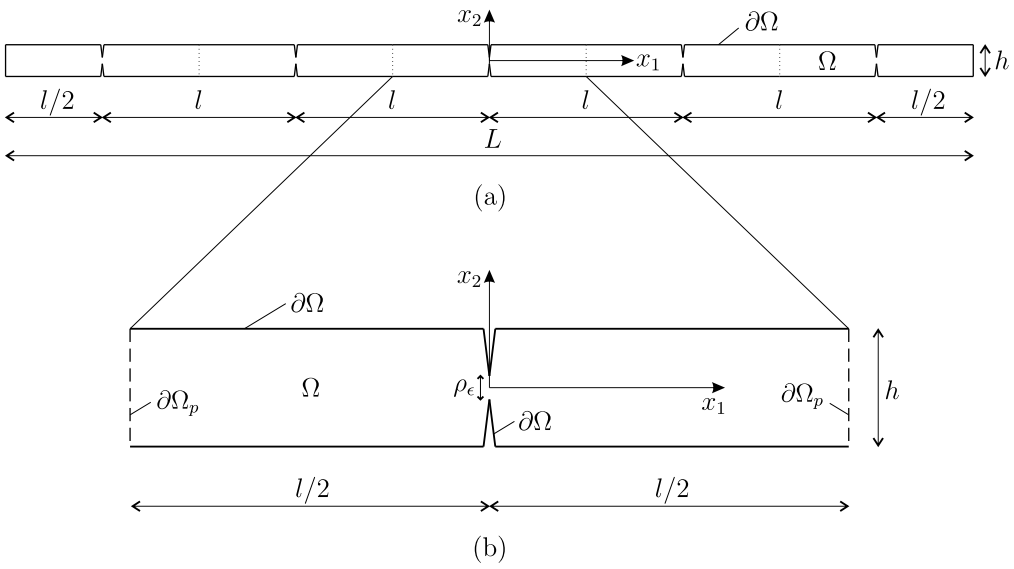

Figure 3. (a) Finite elastic strip with equispaced transverse cracks, that consists of five repeating cells; (b) detail of a repetitive cell. In the figures, Ω represents the interior domain of the strip, $\partial\Omega$ is its traction-free boundary (in solid line), while $\partial\Omega_p$ indicates the ends of the strip where Floquet-Bloch conditions are applied (in dashed line).

We assume that the strip is elastic and that the boundaries are traction-free. Accordingly, the time-harmonic governing equations for the strip are the following:

$$\mu\nabla^2\mathbf{U}(\mathbf{x}) + (\lambda+\mu)\nabla\nabla\cdot\mathbf{U}(\mathbf{x}) + \rho\omega^2\mathbf{U}(\mathbf{x}) = \mathbf{0} \text{ in } \Omega; \tag{2.1a}$$

$$\sigma^{(\mathbf{n})}[\mathbf{U}](\mathbf{x}) = \mathbf{0} \text{ on } \partial\Omega. \tag{2.1b}$$

Here, $\mathbf{x}$ is the position vector, $\mathbf{U}$ is the displacement vector, λ and μ are Lamé coefficients, ρ is the mass density, ω is the radian frequency and σ is the traction vector associated with the unit outward normal $\mathbf{n}$. Furthermore, Ω and $\partial\Omega$ are the interior and the traction-free boundary of the strip, respectively, as indicated in Fig. 3a.

By performing finite element computations in Comsol Multiphysics (version 4.3) to solve numerically Eqs. (2.1), we find the eigenfrequencies and eigenmodes of finite strips with different lengths. The values of the eigenfrequencies and the shapes of some eigenmodes are shown in Fig. 4, where the number of cells varies from 2 to 10. We point out that we have disregarded the eigenfrequencies corresponding to longitudinal motion, which are not relevant in this work. Also, the crosses on the horizontal axis of Fig. 4 represent rigid-body motions, which are not of particular interest.

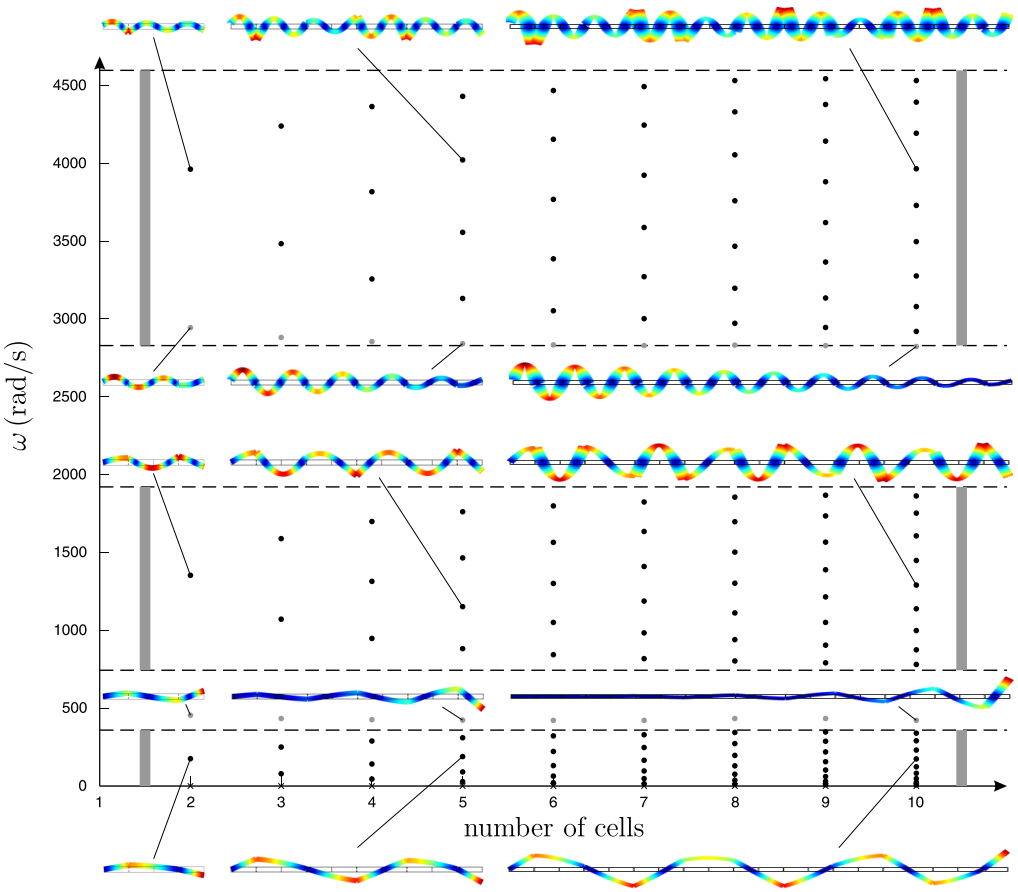

Figure 4. Eigenfrequencies of finite strips possessing different lengths. The horizontal dashed lines represent the boundaries of the band-gaps for the infinite periodic strip, while the propagation bands are shown in grey colour on the sides of the diagram. Some eigenmodes of the finite strips are also reported in the figure. The following set of parameters has been used for the computations: Young's modulus $E = 200\,\mathrm{GPa}$, Poisson's ratio $\nu = 0.3$, mass density $\rho = 7800\,\mathrm{kg/m^3}$, length of the repeating cell $l = 2\,\mathrm{m}$, strip height $h = l/10 = 0.2\,\mathrm{m}$, depth of the cracked section $\rho_\epsilon = h/5 = 0.04\,\mathrm{m}$. (Online version in colour.)

The eigenmodes corresponding to the eigenfrequencies indicated by grey dots exhibit localisation, while those obtained from the eigenfrequencies coloured in black do not have decaying amplitudes. The latter eigenfrequencies increase in number as the number of cells is increased; however, they remain confined within specific ranges of frequency. In the next section, we identify such frequency ranges from the study of the dispersion properties of a periodic strip.

(b) Dispersion properties of the periodic strip

We examine a strip of infinite length, consisting of a periodic array of cells, one of which is shown in Fig. 3b. The top and bottom boundaries of the cell and the sides of the crack are traction-free, while the vertical sides of the cell are subjected to Floquet-Bloch conditions. The equations of motion of the infinite periodic strip result to be:

$$\mu\nabla^2\mathbf{U}(\mathbf{x}) + (\lambda+\mu)\nabla\nabla\cdot\mathbf{U}(\mathbf{x}) + \rho\omega^2\mathbf{U}(\mathbf{x}) = \mathbf{0} \text{ in } \Omega; \tag{2.2a}$$

$$\sigma^{(\mathbf{n})}[\mathbf{U}](\mathbf{x}) = \mathbf{0} \text{ on } \partial\Omega; \tag{2.2b}$$

$$\mathbf{U}(x_1, x_2) = \mathbf{U}(x_1 - l, x_2)\, \mathrm{e}^{\mathrm{i}kl} \text{ on } \partial\Omega_p. \tag{2.2c}$$

In the equations above, Ω is the interior domain of the cell, $\partial\Omega$ is its traction-free boundary, while $\partial\Omega_p$ indicates the ends of the cell where Floquet-Bloch conditions are imposed (see Fig. 3b). Furthermore, k stands for the wavenumber.

We solve Eqs. (2.2) numerically by developing a finite element model in Comsol Multiphysics. In particular, we determine the dispersion curves plotted in Figs. 5a and 5b, which refer to a larger and a smaller value of the cracked section depth ρ_ϵ, respectively. We stress that the numerical data shown in Figs. 5a and 5b are relative to transverse waves and are independent of the strip thickness. In fact, the finite element code also provides the dispersion curves relevant to longitudinal waves; however, the latter are not reported in the figures for clarity's sake.

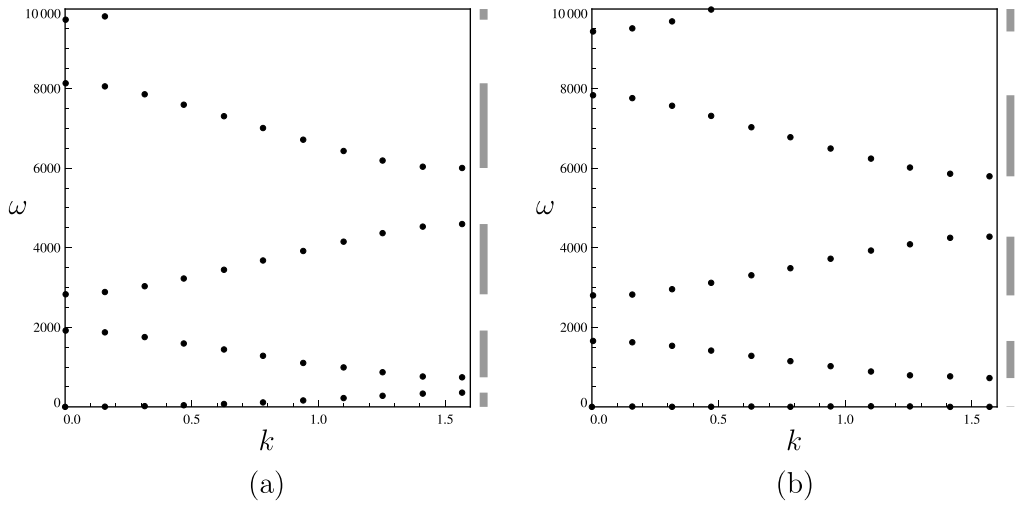

Figure 5. Dispersion curves of the infinite periodic strip for $\rho_\epsilon/h = 1/5$ (a) and $\rho_\epsilon/h = 1/100$ (b), obtained from the finite element software Comsol Multiphysics. The propagation zones are indicated in grey colour on the right of the figures. As for Fig. 4, we have taken $E = 200\,\mathrm{GPa}$, $\nu = 0.3$, $\rho = 7800\,\mathrm{kg/m^3}$, $l = 2\,\mathrm{m}$, $h = l/10 = 0.2\,\mathrm{m}$.

From Figs. 5a and 5b it is apparent that the damage generates bands of non-propagation (band-gaps), which are not present in the intact elastic system. The size of the band-gaps increases at higher level of damage, namely as the depth of the cracked cross-section ρ_ϵ is decreased.

It is interesting to observe that, though the strips considered in Figs. 5a and 5b are nearly disintegrating since ρ_ϵ is small, waves of high frequencies can still propagate in such structures. This is quite a counterintuitive result. Furthermore, by comparing Figs. 5a and 5b we note that the main effect of reducing the depth of the cracked section is to drop the first dispersion curve, which becomes flatter as ρ_ϵ is decreased. On the other hand, the higher dispersion curves are not significantly modified by a change in ρ_ϵ.

The limits of the band-gaps of Fig. 5a are represented by horizontal dashed lines in Fig. 4, in which the same value of ρ_ϵ has been taken into account. We observe that all the eigenfrequencies of the finite strips with different lengths indicated by black dots in Fig. 4, which are relevant to non-localised modes, lie within the propagation bands of the periodic structure (a similar conclusion was drawn in [14] for mono-coupled systems and in [15] for the analysis of a real bridge structure). On the contrary, the eigenmodes corresponding to the eigenfrequencies falling outside the propagation bands of the periodic structure, indicated by grey dots in Fig. 4, are localised near a boundary. Thus, we have shown that it is possible to identify the attainable ranges of the eigenfrequencies of the finite structure by studying the dispersion properties of the infinite periodic structure.

The periodic structure exhibits standing waves at the limits of the band-gaps, where the dispersion curves are flat ($\partial\omega/\partial k = 0$). The lowest eight modes relative to these standing waves, as in Fig. 5b, are plotted in Fig. 6. Modes (a), (c), (e) and (g) show a slope discontinuity at the cracked section, while modes (b), (d), (f) and (h) present a relative displacement in correspondence of the damaged section.

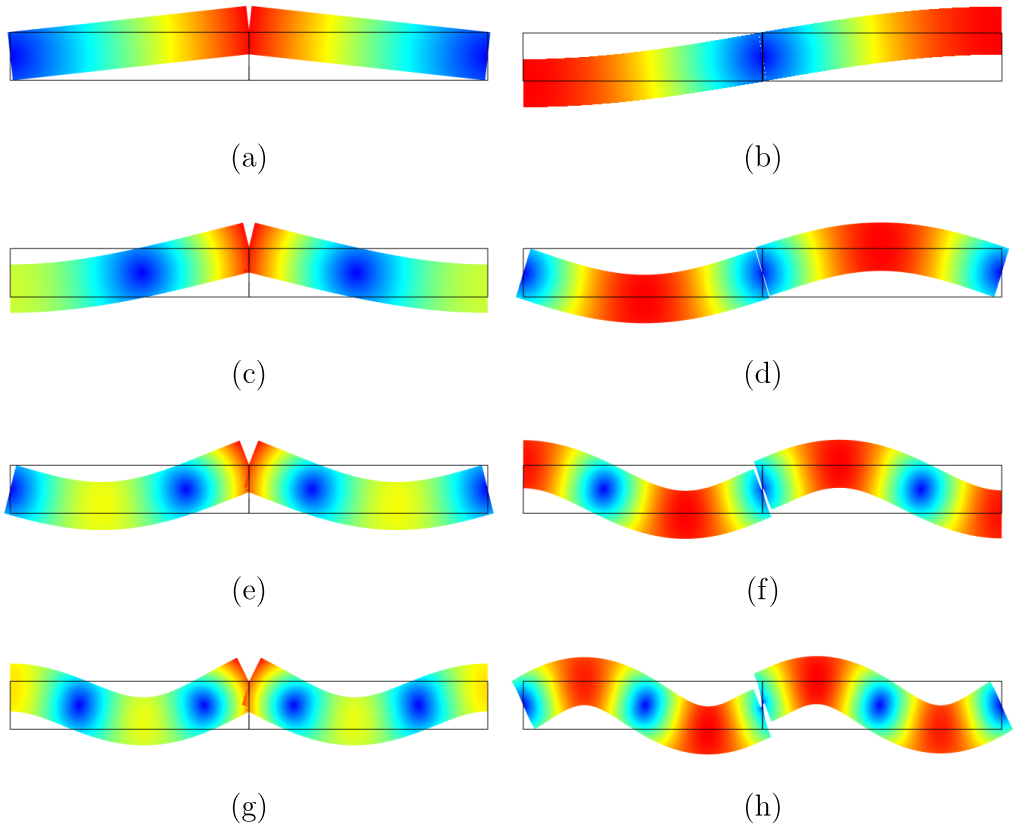

Figure 6. First eight modes (at increasing eigenfrequencies) relative to the standing waves (see Fig. 5b) at $k = \pi/l$ ((a), (b), (e), (f)) and $k = 0$ ((c), (d), (g), (h)), provided by the finite element code. In this case, we have assigned to the geometric and constitutive quantities the same values considered in Fig. 5b ($\rho_\epsilon/h = 1/100$). (Online version in colour.)

In concluding this section, we remark that we have solved numerically the two-dimensional problems defined by Eqs. (2.1) and (2.2). In the next section, we investigate a lower-dimensional model, which allows to derive analytically an efficient approximation of the dynamic properties of the two-dimensional model.

3. Asymptotic reduced beam model

In this section we study a reduced model, represented by a beam with cracked cross-sections that are modelled as elastic junctions. The effective bending (rotational) and shear (translational) stiffnesses of the elastic junctions are denoted as K_b and K_s, respectively. The beam is of infinite length and the damaged cross-sections are located at regular intervals. A periodic segment of the beam is sketched in Fig. 7.

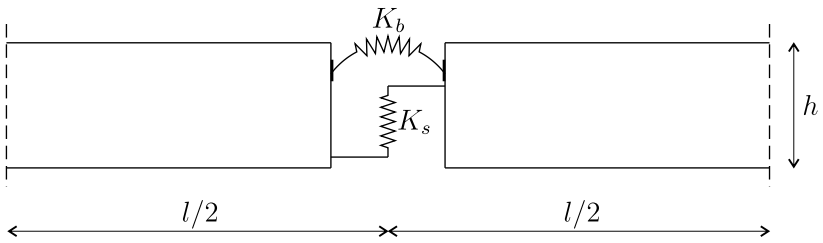

Figure 7. Periodic cell of a beam with elastic connections. The distance along the beam axis between two consecutive elastic connections is constant and equal to l. K_b is the bending stiffness, while K_s is the shear stiffness.

(a) Effective junction conditions

The notion of effective junction conditions was introduced in the book [16]. In the asymptotic models involving boundary layers near singularly perturbed boundaries that encompass connection of several bodies, these are equivalent to conditions of decay of boundary layers away from the relevant junction region. Asymptotic analysis relevant to our model engages effective bending and shear stiffnesses that were determined for the two-dimensional, nearly disintegrating strip shown in Fig. 8. This technique has been applied to asymptotic models of disintegrating solids in [11] for longitudinal loads and in [12] for flexural loads. In these papers, the attention was devoted to static problems, while here we describe the corresponding generalisation to the time-harmonic regime.

Two classes of boundary conditions for a bending problem are analysed: symmetric rotations q at the boundaries (Fig. 8a) and antisymmetric displacements p at the two ends (Fig. 8b). For symmetry, only the half domain $\Omega_\epsilon = \left\{\mathbf{x} \in \mathbb{R}^2 : 0 \le x_1 \le l, |x_2| \le h/2\right\}$ is considered. As far as the bending problem with symmetric rotations is concerned, after the introduction of the scaled spatial variables $\xi_j = x_j/\epsilon$, the displacement vector $\mathbf{u}_\epsilon$ admits the asymptotic approximation [17]

$$\mathbf{u}_\epsilon \approx \epsilon^{-2}\mathbf{u}^{(0)} + \epsilon^{-1}\mathbf{u}^{(1)} + \mathbf{u}^{(2)} + \epsilon\,\mathbf{u}^{(3)} + \epsilon^2\mathbf{U} + \mathbf{L}_\epsilon, \tag{3.1}$$

where $\mathbf{u}^{(i)}$ (i = 0,1,2,3) and $\mathbf{U}$ are functions of (x_1, ξ_2, t), while the boundary layer terms $\mathbf{L}_\epsilon$ are functions of the scaled variables (ξ_1, ξ_2) and decay away from the singularly perturbed boundary that also includes the junction region. The leading order term $\mathbf{u}^{(0)}$ has the form $(0, u_2^{(0)}(x_1)\,\mathrm{e}^{\mathrm{i}\omega t})$ and satisfies the following differential equation:

$$\frac{h^3}{12}\frac{4\mu(\lambda+\mu)}{(\lambda+2\mu)}u_2^{(0)\prime\prime\prime\prime}(x_1) - \rho h\,\omega^2 u_2^{(0)}(x_1) = 0. \tag{3.2}$$

The latter can also be derived as the solvability condition of a Neumann problem on the cross-section of the strip for $\mathbf{U}$, as discussed in [17]. Eq. (3.2) has the structure of a beam equation of motion and requires four boundary conditions, which are determined from the analysis of the conditions of decay for the corresponding boundary layers. The conditions at the right end of the

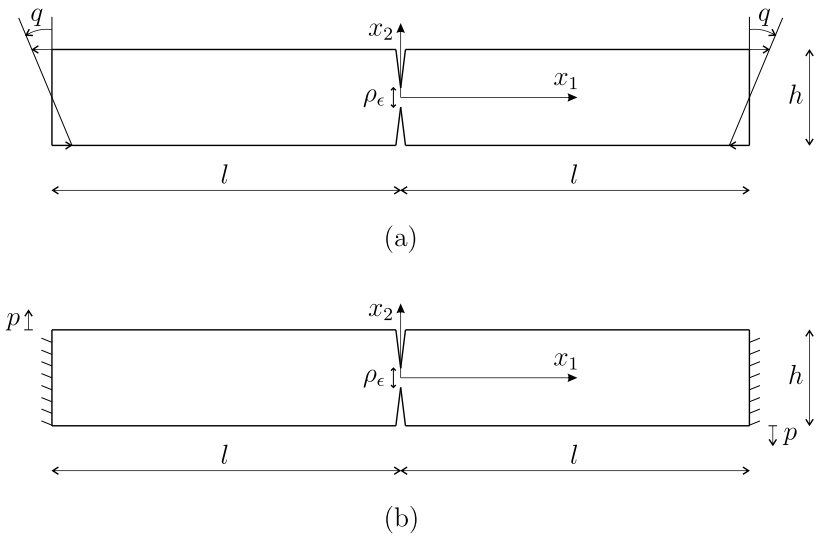

Figure 8. Elastic strip subjected to symmetric rotations (a) and antisymmetric displacements (b) at the ends.

domain are:

$$u_2^{(0)}(l) = 0; \tag{3.3}$$

$$u_2^{(0)\prime}(l) = -q. \tag{3.4}$$

Correspondingly, as shown in [12] the remaining conditions at the left end have the form:

$$u_2^{(0)\prime\prime\prime}(0) = 0, \tag{3.5}$$

$$u_2^{(0)\prime}(0) - \frac{5-2\nu}{6\pi(1-\nu)}\frac{h^3}{\rho_\epsilon^2}u_2^{(0)\prime\prime}(0) = 0. \tag{3.6}$$

The second derivative $u_2^{(0)\prime\prime}(0)$ represents the curvature at $x_1 = 0$, while the first derivative $u_2^{(0)\prime}(0)$ is equal to half of the rotation $\Delta\varphi$ at the junction. By using the relationship between bending moment (per unit thickness) M and curvature $u_2^{(0)\prime\prime}(0)$, given by

$$M = \frac{E\,h^3}{12(1-\nu^2)}u_2^{(0)\prime\prime}(0), \tag{3.7}$$

the rotational stiffness (per unit thickness s) $\bar{K}_b = M/\Delta\varphi$ is found:

$$\bar{K}_b = \frac{K_b}{s} = \frac{\pi E\rho_\epsilon^2}{4\,(5-2\nu)\,(1+\nu)}. \tag{3.8}$$

We remind that E is Young's modulus, while ν is Poisson's ratio.

A similar procedure can be applied to the bending problem with antisymmetric displacements, from which the following expression of the translational stiffness (per unit thickness) is derived (see [12] for details):

$$\bar{K}_s = \frac{K_s}{s} = \frac{\pi E}{4\,(1-\nu^2)}\frac{1}{\log\left(\frac{h}{\rho_\epsilon}\right)}. \tag{3.9}$$

The analysis of [12] has illustrated that the expressions (3.8) and (3.9) provided a sufficiently high accuracy for $0 < \rho_\epsilon/h \leq 0.35$. In the following sections, we will discuss Eqs. (3.8) and (3.9) being applied to dynamic problems, in particular to describe the junction conditions of a periodic beam subjected to flexural waves.

(b) Dispersion properties of the asymptotic reduced model

We use the transfer matrix method to obtain the propagation and non-propagation zones for the periodic beam with elastic connections. The transfer matrix is a mathematical tool that can be efficiently implemented to analyse periodic media, both in electromagnetism (e.g. [18]) and in elasticity (e.g. [19]). It allows to define the vector of generalised displacements and generalised forces at the end of a periodic cell in terms of the same vector at the beginning of the cell. Examples for mono-coupled elastic periodic structures can be found in [14,19–21]. In the present case, the structure is a bi-coupled system, because there are two degrees of freedom, i.e. vertical displacement and rotation. The corresponding generalised forces are bending moment and shear. Therefore, the transfer matrix has dimensions 4x4 independently of the complexity of the periodic cell. Different instances of bi-coupled periodic structures are investigated in [22,23]. In the case examined in this paper, the transfer matrix can be written in compact form as

$$\mathbf{M} = \mathbf{M_{int}}\,(\mathbf{I} + \mathbf{K})\,. \tag{3.10}$$

$\mathbf{M_{int}}$ is the transfer matrix of an intact beam of period l [23]:

$$\mathbf{M_{int}} = \begin{bmatrix} \frac{\cos(\beta l)+\cosh(\beta l)}{2} & \frac{\sin(\beta l)+\sinh(\beta l)}{2\beta} & \frac{\cos(\beta l)-\cosh(\beta l)}{2\beta^2 EJ} & \frac{\sin(\beta l)-\sinh(\beta l)}{2\beta^3 EJ} \\ \frac{\beta[-\sin(\beta l)+\sinh(\beta l)]}{2} & \frac{\cos(\beta l)+\cosh(\beta l)}{2} & -\frac{\sin(\beta l)+\sinh(\beta l)}{2\beta EJ} & \frac{\cos(\beta l)-\cosh(\beta l)}{2\beta^2 EJ} \\ \frac{\beta^2 EJ[\cos(\beta l)-\cosh(\beta l)]}{2} & \frac{\beta EJ[\sin(\beta l)-\sinh(\beta l)]}{2} & \frac{\cos(\beta l)+\cosh(\beta l)}{2} & \frac{\sin(\beta l)+\sinh(\beta l)}{2\beta} \\ \frac{-\beta^3 EJ[\sin(\beta l)+\sinh(\beta l)]}{2} & \frac{\beta^2 EJ[\cos(\beta l)-\cosh(\beta l)]}{2} & \frac{\beta[-\sin(\beta l)+\sinh(\beta l)]}{2} & \frac{\cos(\beta l)+\cosh(\beta l)}{2} \end{bmatrix}, \tag{3.11}$$

where $\beta = (\rho A\omega^2/EJ)^{1/4}$, ω is the radian frequency, while A and J are respectively the area and the second moment of inertia of the beam cross-section. Furthermore, the matrix $\mathbf{I}$ appearing in Eq. (3.10) represents the 4x4 identity matrix, while $\mathbf{K}$ is the "stiffness matrix" given by

$$\mathbf{K} = \begin{bmatrix} 0 & 0 & 0 & \frac{1}{K_s} \\ 0 & 0 & -\frac{1}{K_b} & 0 \\ 0 & 0 & 0 & 0 \\ 0 & 0 & 0 & 0 \end{bmatrix}. \tag{3.12}$$

By imposing Bloch-Floquet conditions we find the dispersion relation, which is given by

$$\det\left(\mathbf{M} - \mathrm{e}^{\mathrm{i}kl}\mathbf{I}\right) = 0, \tag{3.13}$$

where k is the wavenumber.

If the stiffnesses K_b and K_s are chosen arbitrarily, the dynamic problem can be described by three non-dimensional parameters:

$$\phi = \beta\, l = \sqrt[4]{\frac{\rho A\omega^2}{EJ}}\, l; \tag{3.14a}$$

$$\kappa_b = \frac{K_b l}{EJ}; \tag{3.14b}$$

$$\kappa_s = \frac{K_s l^3}{EJ}. \tag{3.14c}$$

ϕ is a non-dimensional parameter related to frequency, which will be henceforth referred to as "frequency parameter". κ_b and κ_s represent the normalisations of the junction stiffnesses with respect to the flexural rigidity of the beam; they can be indicated as "effective damage parameters".

The unimodular transfer matrix $\mathbf{M}$ is characterised by two independent invariants, which are expressed in terms of the frequency and effective damage parameters in Eqs. (3.14) as follows:

$$I_1 = 2\left[\cos(\phi) + \cosh(\phi)\right] + \frac{\phi}{2}\left[\left(\frac{1}{\kappa_b} - \frac{\phi^2}{\kappa_s}\right)\sinh(\phi) - \left(\frac{1}{\kappa_b} + \frac{\phi^2}{\kappa_s}\right)\sin(\phi)\right]; \tag{3.15a}$$

$$\begin{aligned} I_2 =& \frac{1}{2}\left[4 + \frac{\phi^4}{\kappa_b\kappa_s} + \left(8 - \frac{\phi^4}{\kappa_b\kappa_s}\right)\cos(\phi)\cosh(\phi)\right] \\ &+ \phi\left[\left(\frac{1}{\kappa_b} - \frac{\phi^2}{\kappa_s}\right)\cos(\phi)\sinh(\phi) - \left(\frac{1}{\kappa_b} + \frac{\phi^2}{\kappa_s}\right)\sin(\phi)\cosh(\phi)\right]. \end{aligned} \tag{3.15b}$$

The invariants are useful to distinguish the ranges of frequency in which the waves propagate ("propagation zones") and where waves are evanescent ("non-propagation zones"). In [22] it is shown that for bi-coupled periodic systems, such as beams, the propagation zones can be classified into four types: the pass-pass zones, where two waves propagate without attenuation in each direction; the pass-stop zones, where one wave propagates and the other wave decays exponentially; the stop-stop zones, where both waves decay exponentially; and the complex zones, which are special stop-stop zones that are characterised by complex conjugate eigenvalues with non-unit modulus. These four zones are separated in the plane of the invariants I_1 and I_2 by the following three curves:

$$f_1(I_1, I_2): \; I_2 = 2I_1 - 2; \tag{3.16a}$$

$$f_2(I_1, I_2): \; I_2 = -2I_1 - 2; \tag{3.16b}$$

$$f_3(I_1, I_2): \; I_2 = \frac{1}{4}I_1^2 + 2. \tag{3.16c}$$

f_1 and f_2 represent straight lines, while f_3 is a parabola. By introducing Eqs. (3.15) into Eqs. (3.16), we determine the boundaries of the propagation zones in the space defined by the three non-dimensional parameters (3.14), which will be henceforth referred to as "physical space".

By fixing the constitutive properties of the material (E, ν, ρ) and evaluating the stiffnesses K_b and K_s by means of Eqs. (3.8) and (3.9), we reduce the non-dimensional parameters that fully characterise the problem to two: the frequency parameter ϕ, defined by Eq. (3.14*a*), and the ratio ρ_ϵ/h. As a consequence, the physical space reduces to a plane. The propagation zones for a particular choice of the material properties are shown in Fig. 9. In this diagram, the grey and white regions represent the pass-stop and the stop-stop zones, respectively. We observe that there are no pass-pass nor complex zones in the ranges of values considered.

We determine the dispersion curves from Eq. (3.13) for the cases $\rho_\epsilon = h/5$ and $\rho_\epsilon = h/100$, which are plotted in solid thick black lines in Figs. 10a and 10b, respectively. In the same figures, the solid grey lines represent the dispersion curves of an intact beam, which can also be derived from Eq. (3.13) by taking $K_b, K_s \to \infty$.

We note that waves of any frequency can travel in an intact beam (see also [24], Section 3). In such a case, the dispersion curves are straight lines in the $(\phi, k\,l)$ space. If the beam contains cracks, instead, non-propagation bands appear. The upper limit of the lowest stop-stop band is independent of the value of ρ_ϵ and coincides with the lowest value that the dispersion curves of an intact beam attain at $k\,l = \pi$; on the other hand, its lower limit decreases as the crack grows, as expected on physical ground. As already detailed in Fig. 5, it is evident that the "amount of damage" strongly influences the acoustic pass-band, while it has a less relevant effect on the optical pass-bands.

(c) Efficiency of the asymptotic approximation

The dynamic properties of the two-dimensional strip model, derived numerically in Section 2, can be predicted with good accuracy by the reduced beam model in a finite range of frequencies.

In Figs. 11a and 11b we compare the analytical dispersion curves, obtained from the transfer matrix method applied to the periodic beam, with the numerical values provided by Comsol Multiphysics for the periodic strip, for the cases $\rho_\epsilon/h = 1/5$ and $\rho_\epsilon/h = 1/100$ respectively.

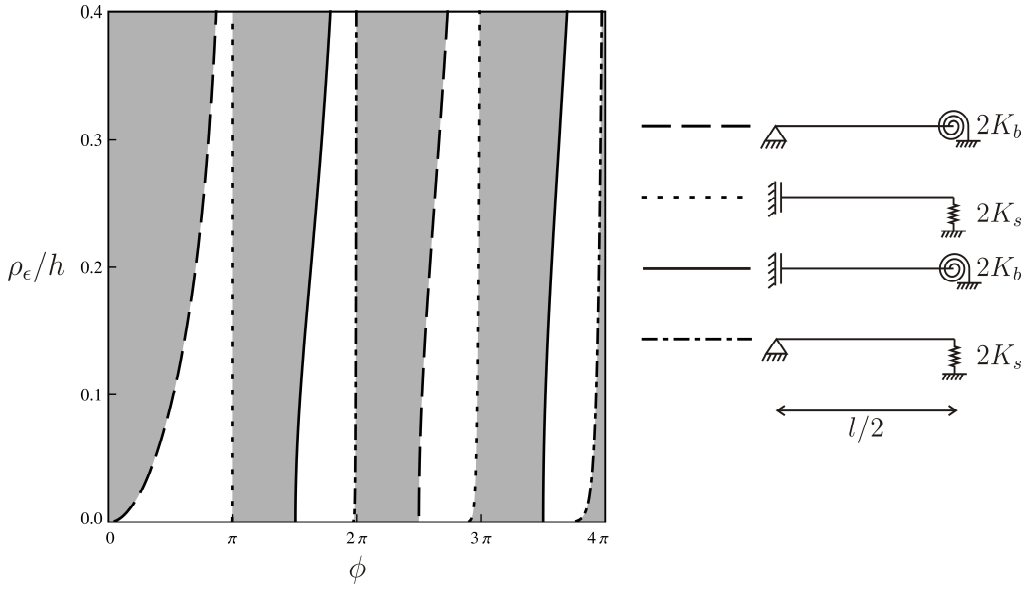

Figure 9. Physical plane representation of the propagation zones. Grey regions: pass-stop zones; white regions: stop-stop zones. The limits of the propagation zones can also be obtained from the eigenfrequencies of the simple beams with appropriate boundary conditions sketched on the right of the figure, as detailed in Section (d). ($E = 200\,\mathrm{GPa}$, $\nu = 0.3$, $\rho = 7800\,\mathrm{kg/m^3}$, $h = 0.2\,\mathrm{m}$.)

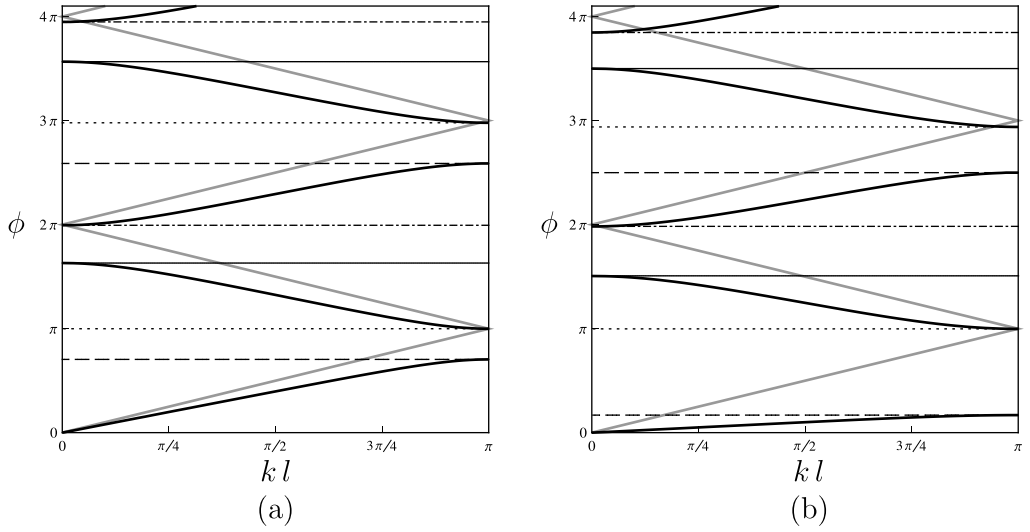

Figure 10. Dispersion curves for an intact beam (solid grey lines) and for a damaged beam (solid thick black lines) with $\rho_\epsilon = h/5$ (a) and $\rho_\epsilon = h/100$ (b). The horizontal lines are determined from the eigenfrequencies of the simple beams depicted on the right of Fig. 9. ($E = 200\,\mathrm{GPa}$, $\nu = 0.3$, $\rho = 7800\,\mathrm{kg/m^3}$, $h = 0.2\,\mathrm{m}$.)

From Figs. 11a and 11b it can be seen that there is a very good agreement between the first three analytical dispersion curves and the numerical findings. At higher frequencies, the discrepancy between the two models increases. We stress the fact that two approximations are embedded into the damaged beam model: the reduced one-dimensional model with respect to the continuous

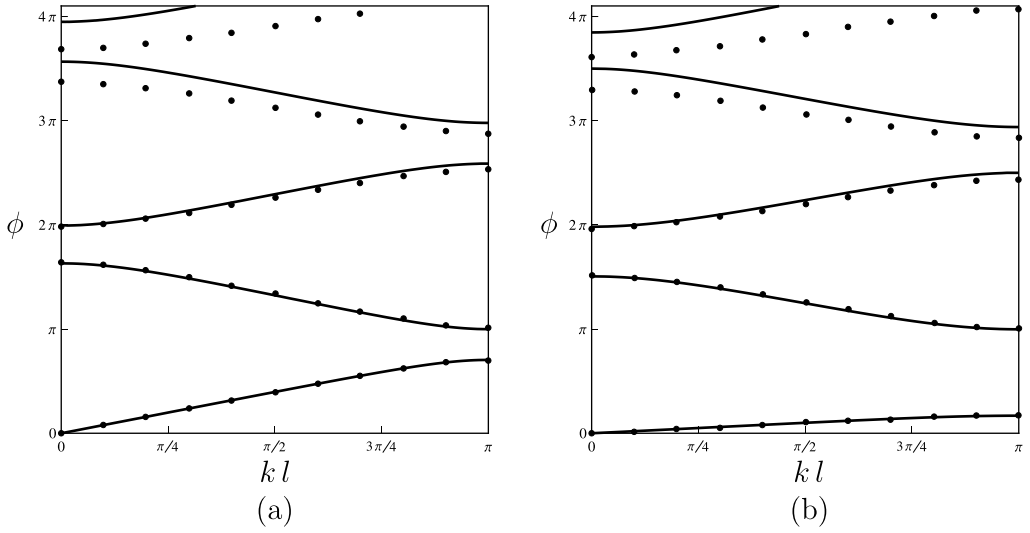

Figure 11. Non-dimensional frequency parameter ϕ versus normalised wavenumber $k\,l$ for $\rho_\epsilon/h = 1/5$ (a) and $\rho_\epsilon/h = 1/100$ (b). The solid lines represent the solutions of Eq. (3.13) applied to the beam model, while the dots are the numerical data calculated for the strip model (same as in Fig. 5, but in different coordinates). ($E = 200\,\mathrm{GPa}$, $\nu = 0.3$, $\rho = 7800\,\mathrm{kg/m^3}$, $h = 0.2\,\mathrm{m}$.)

two-dimensional one, and the asymptotic approximation for the effective junction conditions. Analogous computations for an intact beam show similar discrepancies between the continuous and the structural beam model. These computations, not reported here for brevity, also indicate that the validity frequency range of the one-dimensional model is wider as the slenderness of the unit cell is increased. These results show that the effective junction conditions are efficient within the frequency range where the beam model is valid.

(d) Standing waves. Analytical estimates of the band-gap boundaries

In this section we give simple analytical expressions for the limits of the band-gaps. These can be obtained by computing the eigenfrequencies of simple beam models, whose boundary conditions can be deduced from the standing waves reported in Fig. 6.

The standing waves obtained for $k\,l = \pi$ at the lower limits of the stop-stop zones (Figs. 6a and 6e) are identical to the eigenmodes of a simple beam simply supported at one end and with a rotational spring (of stiffness $2K_b$) at the other end, that is sketched in Fig. 12a. In this figure, the dashed lines represent the first two eigenmodes. The normalised eigenfrequencies of this simple beam can be calculated from the following implicit equation:

$$\cosh\left(\frac{\phi}{2}\right)\left[4\kappa_b\cos\left(\frac{\phi}{2}\right)-\phi\sin\left(\frac{\phi}{2}\right)\right]+\sinh\left(\frac{\phi}{2}\right)\left[\phi\cos\left(\frac{\phi}{2}\right)\right]=0. \tag{3.17}$$

We remind that ϕ is proportional to the square root of the frequency and it is a non-dimensional quantity; therefore, we denote ϕ as "normalised eigenfrequency".

On the other hand, the standing waves computed for $k\,l = \pi$ at the upper limits of the stop-stop zones (Figs. 6b and 6f) have the same shapes of the eigenmodes of a simple beam with a guided support at one end and a translational spring (of stiffness $2K_s$) at the other end, shown in Fig. 12b. The normalised eigenfrequencies of this simple beam can be determined from the following equation:

$$\cosh\left(\frac{\phi}{2}\right)\left[-4\kappa_s\cos\left(\frac{\phi}{2}\right)+\phi^3\sin\left(\frac{\phi}{2}\right)\right]+\sinh\left(\frac{\phi}{2}\right)\left[\phi^3\cos\left(\frac{\phi}{2}\right)\right]=0. \tag{3.18}$$

The first two eigenmodes are plotted in dashed lines in Fig. 12b.

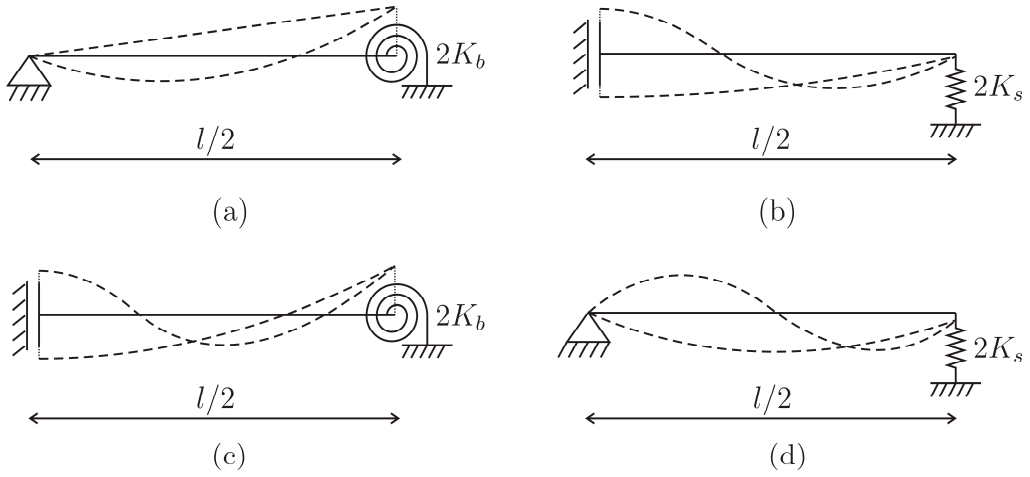

Figure 12. Lowest two eigenmodes of simple beams with different boundary conditions. The corresponding normalised eigenfrequencies are calculated by solving (a) Eq. (3.17), (b) Eq. (3.18), (c) Eq. (3.19) and (d) Eq. (3.20).

The standing waves at $k\,l = 0$, determined at the beginnings of the stop-stop zones (Figs. 6c and 6g) and at the ends of the stop-stop zones (Figs. 6d and 6h), resemble the eigenmodes of the simple beams drawn in Figs. 12c and 12d, respectively. The corresponding normalised eigenfrequencies can be found from the following equations:

$$\cosh\left(\frac{\phi}{2}\right)\left[\phi\sin\left(\frac{\phi}{2}\right)\right]+\sinh\left(\frac{\phi}{2}\right)\left[4\kappa_b\sin\left(\frac{\phi}{2}\right)+\phi\cos\left(\frac{\phi}{2}\right)\right]=0; \tag{3.19}$$

$$\cosh\left(\frac{\phi}{2}\right)\left[\phi^3\sin\left(\frac{\phi}{2}\right)\right]-\sinh\left(\frac{\phi}{2}\right)\left[4\kappa_s\sin\left(\frac{\phi}{2}\right)+\phi^3\cos\left(\frac{\phi}{2}\right)\right]=0. \tag{3.20}$$

From the above considerations, it can be concluded that the limits of the stop-stop zones can be evaluated analytically from the eigenfrequencies of simple structures. This approach is easier than solving the dispersion relation of a periodic structure. The normalised eigenfrequencies of the beams sketched in Figs. 12a-12d are plotted in Figs. 9 and 10 in dashed, dotted, solid and dot-dashed black lines, respectively. Especially Fig. 9 shows that the limits of the stop-stop zones coincide with the solutions of Eqs. (3.17)-(3.20).

The transcendental equations (3.17)-(3.20) can be expanded in Taylor series for $\phi = 0$ in order to find an approximation to their exact solution. Accordingly, the first solution of equations (3.17)-(3.20), which depends on either κ_b or κ_s, is approximated with high accuracy by, respectively:

$$\phi_1=\phi_1(\kappa_b)=2\sqrt[4]{6\frac{\kappa_b}{2+\kappa_b}}; \tag{3.21a}$$

$$\phi_1=\phi_1(\kappa_s)=2\sqrt[4]{6\frac{840+35\kappa_s-\sqrt{105}\sqrt{6720+336\kappa_s+11\kappa_s^2}}{336+\kappa_s}}; \tag{3.21b}$$

$$\phi_1=\phi_1(\kappa_b)=2\sqrt{3}\sqrt[4]{10\frac{21+7\kappa_b-\sqrt{7}\sqrt{53+30\kappa_b+5\kappa_b^2}}{5+\kappa_b}}; \tag{3.21c}$$

$$\phi_1=\phi_1(\kappa_s)=2\sqrt{3}\sqrt[4]{10\frac{840+7\kappa_s-\sqrt{35}\sqrt{20160+48\kappa_s+\kappa_s^2}}{720+\kappa_s}}. \tag{3.21d}$$

We plot the approximations (3.21a)-(3.21d) in dashed black colour in Figs. 13a-13d, respectively. In the same figures, the solid grey lines represent the exact solutions obtained from Eqs. (3.17)-(3.20), showing the excellent agreement with the approximated solutions (3.21). We point out that we have considered a wider range of values for κ_s, since κ_s is generally larger than κ_b for a given ρ_ϵ. All functions increase monotonically with the stiffness on which they depend.

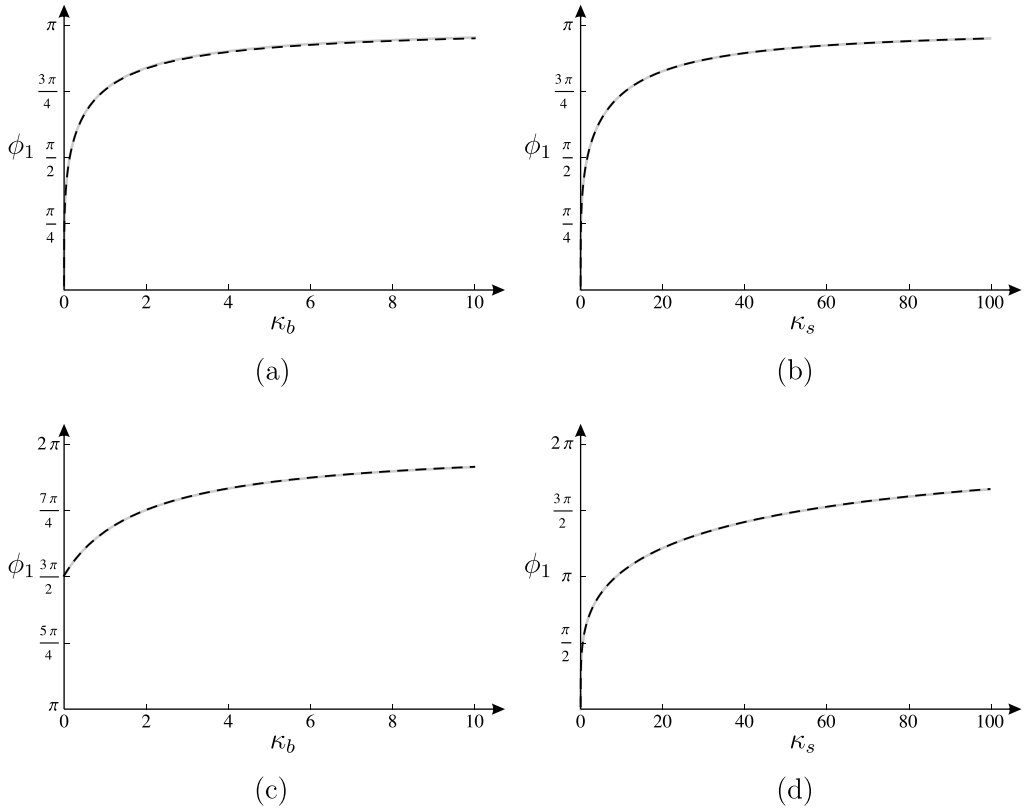

Figure 13. First normalised eigenfrequency, as a function of the corresponding normalised stiffness, of the beams shown in Fig. 12. Dashed black lines: approximations derived from Eqs. (3.21a)-(3.21d); solid grey lines: exact solutions determined from Eqs. (3.17)-(3.20).

4. Conclusions

In this paper, we have examined the propagation of transverse waves in a two-dimensional elastic strip with distributed cracks. Numerical simulations concerning infinite periodic strips have shown that band-gaps arise as a consequence of the cracks present in the structure, and the limits of the band-gaps depend on the depth of the cracked sections. If, instead, the strips are of finite length, the eigenfrequencies of non-localised modes fall within well identified frequency intervals, coinciding with the pass-band of the periodic structure. The number of eigenfrequencies of the finite structure in each pass-band is shown to increase linearly with the number of cells composing the system.

In order to predict the positions and the sizes of the band-gaps for a strip with a periodic damage, we have developed a lower-dimensional periodic beam model, in which the cracked sections are represented by elastic junctions with a bending and a shear spring. The effective rotational and translational stiffnesses are derived by means of an asymptotic analysis. A

comparison with the numerical findings obtained from the two-dimensional model has shown that the lowest band-gaps of the strip can be determined with a high level of accuracy from the dispersion curves of the periodic beam.

The limits of the band-gaps coincide with the eigenfrequencies of simple beams, whose boundary conditions have been deduced from the shapes of the standing waves of the elastic strip. This result is very important in practice, since the determination of the eigenfrequencies of simple beams is more straightforward than the solution of the dispersion relation of a periodic structure.

The results of this work can be used to design systems with filtering properties, and to detect and possibly estimate quantitatively the presence of cracks inside structural and mechanical elements by means of non-destructive techniques.

Acknowledgment

G.C. and M.B. wish to acknowledge the financial support of the Regione Autonoma della Sardegna (LR7 2010, grant 'M4' CRP-27585). M.B. and A.B.M. acknowledge the financial support of the European Community's Seven Framework Programme under contract number PIEF-GA-2011-302357-DYNAMETA.

References

1. Movchan, A.B. & Slepyan, L.I. 2007 Band gap Green's functions and localized oscillations. Proc. R. Soc. A **463**, 2709-2727. (DOI 10.1098/rspa.2007.0007)
2. McPhedran, R.C., Movchan, A.B. & Movchan, N.V. 2009 Platonic crystals: Bloch bands, neutrality and defects. Mech. Mat. **41**, 356-363. (DOI 10.1016/j.mechmat.2009.01.005)
3. Poulton C.G., Movchan A.B., Movchan N.V. & McPhedran, R.C. 2012 Analytic theory of defects in periodically structured elastic plates. Proc. R. Soc. A **468**, 1196-1216. (DOI 10.1098/rspa.10.1098/rspa.2011.0609)
4. Mishuris, G.S., Movchan, A.B. & Slepyan, LI 2009 Localization and dynamic defects in lattice structures. In: *Computational and Experimental Mechanics of Advanced Materials (CISM Courses and Lectures)*, vol. 514, pp. 51-82. Wien, Austria: Springer-Verlag.
5. Mishuris, G.S., Movchan, A.B. & Slepyan, LI 2009 Localised knife waves in a structured interface. J. Mech. Phys. Solids **57**, 1958-1979. (DOI 10.1016/j.jmps.2009.08.004)
6. Bigoni, D., Guenneau, S., Movchan, A.B. & Brun, M. 2013 Elastic metamaterials with inertial locally resonant structures: Application to lensing and localization. Phys. Rev. B **87**, 174303. (DOI 10.1103/PhysRevB.87.174303)
7. Carta, G., Jones, I.S., Brun, M., Movchan, N.V. & Movchan, A.B. 2013 Crack propagation induced by thermal shocks in structured media. Int. J. Solids Struct. **50**, 2725-2736. (DOI 10.1016/j.ijsolstr.2013.05.001)
8. Mishuris, G.S., Movchan, A.B. & Bercial, J.P. 2007 Asymptotic analysis of Bloch-Floquet waves in a thin bi-material strip with a periodic array of finite-length cracks. Waves Random Complex Media **17**, 511-533. (DOI 10.1080/17455030701288137)
9. Vellender, A., Mishuris, G.S. & Movchan, A.B. 2011 Weight function in a bimaterial strip containing an interfacial crack and an imperfect interface. Application to Bloch Floquet analysis in a thin inhomogeneous structure with cracks. Multiscale Model. Simul. **9**, 1327-1349. (DOI 10.1137/110824838)
10. Vellender, A. & Mishuris, G.S. 2012 Eigenfrequency correction of Bloch-Floquet waves in a thin periodic bi-material strip with cracks lying on perfect and imperfect interfaces. Wave Motion **49**, 258-270. (DOI 10.1016/j.wavemoti.2011.11.002)

11. Zalipaev, V.V., Movchan, A.B. & Jones, I.S. 2007 Two-parameter asymptotic approximations in the analysis of a thin solid fixed on a small part of its boundary. Quart. J. Mech. Appl. Math. **60**, 457-471. (DOI 10.1093/qjmam/hbm019)
12. Gei, M., Jones, I.S. & Movchan, A.B. 2009 Junction conditions for cracked elastic thin solids under bending and shear. Quart. J. Mech. Appl. Math. **62**, 481-493. (DOI 10.1093/qjmam/hbp017)
13. Ostachowicz, W.M. & Krawczuk, M. 1991 Analysis of the effect of cracks on the natural frequencies of a cantilever beam. J. Sound Vibr. **150**, 191-201. (DOI 10.1016/0022-460X(91)90615-Q)
14. Mead, D.J. 1975 Wave propagation and natural modes in periodic systems: I. Mono-coupled systems. J. Sound Vibr. **40**, 1-18. (DOI 10.1016/S0022-460X(75)80227-6)
15. Brun, M., Giaccu, G.F., Movchan, A.B. & Movchan, N.V. 2012 Asymptotics of eigenfrequencies in the dynamic response of elongated multi-structures. Proc. R. Soc. Lond. A **468**, 378-394. (DOI 10.1098/rspa.2011.0415)
16. Kozlov, V.A., Maz'ya, V.G. & Movchan, A.B. 1999 *Asymptotic Analysis of Fields in Multi-Structures*, Oxford, UK: Oxford University Press.
17. Movchan, A.B. & Movchan, N.V. 1995 *Mathematical Modelling of Solids with Nonregular Boundaries*, Boca Raton, Florida: CRC Press.
18. Lekner, J. 1994 Light in periodically stratified media. J. Opt. Soc. Am. A **11**, 2892-2899. (DOI 10.1364/JOSAA.11.002892)
19. Faulkner, M.G. & Hong, D.P. 1985 Free vibrations of mono-coupled periodic system. J. Sound Vibr. **99**, 29-42. (DOI 10.1016/0022-460X(85)90443-2)
20. Brun, M., Guenneau, S., Movchan, A.B. & Bigoni, D. 2010 Dynamics of structural interfaces: Filtering and focussing effects for elastic waves. J. Mech. Phys. Solids **58**, 1212-1224. (DOI 10.1016/j.jmps.2010.06.008)
21. Carta, G. & Brun, M. 2012 A dispersive homogenization model based on lattice approximation for the prediction of wave motion in laminates. J. Appl. Mech. **79**, 021019. (DOI 10.1115/1.4005579)
22. Romeo, F. & Luongo, A. 2002 Invariants representation of propagation properties for bi-coupled periodic structures. J. Sound Vibr. **257**, 869-886. (DOI 10.1006/jsvi.5065)
23. Carta, G. & Brun, M. Wave propagation properties of periodic systems of beams. In submission.
24. Graff, K.F. 1975 *Wave motion in elastic solids*, London, UK: Oxford University Press.